Systematic dynamic viscoelasticity measurements for chitin nanofibers prepared with various concentrations, disintegration times, acidities, and crystalline structures

Shin Suenaga, Mitsumasa Osada*

Department of Chemistry and Materials, Faculty of Textile Science and Technology, Shinshu University, 3-15-1, Tokida, Ueda, Nagano 386-8567, Japan

*Corresponding author. Tel.: +81-268-21-5458; Fax: +81-268-21-5391

E-mail: osadam@shinshu-u.ac.jp

Abstract

Dynamic viscoelasticities were measured for chitin nanofiber (ChNF) dispersions prepared with various concentrations, disintegration times, acidities, and crystalline structures. The 0.05 w/v% dispersions of pH neutral ChNFs continuously exhibited elastic behavior. The 0.05 w/v% dispersions of acidified ChNFs, on the other hand, transitioned from a colloidal dispersion to a critical gel and then exhibited elastic behavior with increasing ChNF concentration. A double-logarithmic chart of the concentration vs. the storage modulus was prepared and indicated the fractal dimension and the nanostructure in the dispersion. The results determined that the neutral α- and β-ChNFs were dispersed but showed some remaining aggregations and that the acidified β-ChNFs were completely individualized. In addition, the α-chitin steadily disintegrated with increasing disintegration time, and the aspect ratio of the β-chitin decreased as a result of the excessive disintegration. The storage moduli of the ChNFs were greater than those of chitin solutions, nanorods, and nanowhiskers with the same solids concentrations.

Keywords: Chitin nanofiber, Dynamic viscoelasticity measurement, Scaling law

1. Introduction

Chitin nanofibers (ChNFs) are characterized by a high modulus [1], a high relative surface area (i.e., exposure of a large number of hydrophilic functional groups) [2], and an excellent biocompatibility [3]. Although nano sized chitin can be obtained by electrospinning a chitin solution [4] and hydrolyzing the product with an inorganic acid [5], narrow (~10 nm) and long (~1 μm) ChNFs are obtained mainly by wet disintegration [6]. Given their unique mechanical and desirable biological properties, ChNFs have been studied as fillers for plastic materials [7] and scaffolds for cell cultures [8]. To this end, ChNF dispersions have often been converted into hydrogels [9], aerogels [10], and films [11]. Emphasis is placed on the strength or modulus of these materials. The strength of a bulk material would depend on the intrinsic elastic modulus of the NFs, the density of the crosslinking or entanglement points, and the bonding between the NFs (e.g., covalent bonds, hydrogen bonds, electrostatic interaction, etc.). To utilize NFs effectively, therefore, it is important to comprehend the extent of the entanglement of the NFs as well as their rheological properties.

Our previous study revealed that the viscosity of β-ChNFs increased by a factor of around 10 as a result of adding dilute hydrochloric acid before disintegration, while that of α-ChNFs was only slightly affected by the addition of the acid [12]. For a steady shear flow measurement corresponding to a viscoelasticity measurement in the nonlinear region (strain vs. stress), the ChNFs were disentangled; thus, the elasticity can be disregarded. To discuss the nanostructures in ChNF dispersions, a dynamic viscoelasticity measurement should be carried out in the linear region, with particular attention paid to the storage modulus, G'. In dynamic viscoelasticity measurements, the amount of stress is detected for a given strain applied to a sample, the complex elastic modulus (which is a proportionality constant for strain vs. stress) can be determined, and the contribution ratio of the viscosity and elasticity for that constant can be calculated from the phase delay, δ. Here, G' is the stiffness of the viscoelastic fluid resulting

from the entanglement or crosslinking of the network structure, while the loss modulus, G'', is the compliance of the viscoelastic fluid resulting from the energy dissipated owing to the permanent deformation of the polymer [13].

Some studies have reported dynamic viscoelasticity measurements on ChNFs. Yokoi et al. have assumed a liquid-crystalline arrangement of β-ChNFs in an acidic solution, given that the relationship between G' and the solids concentration varies with the sonication duration [14]. Kose et al. have demonstrated the relationship between G' and the disintegration times with a wet disintegration system [15]. However, no studies to date have attempted systematic dynamic viscoelasticity measurements that consider the disintegration times, solids concentration, and the presence or absence of acid for either α- or β-ChNFs. In the present study, ChNF dispersions were prepared for different disintegration conditions of both α- and β-chitin crystalline structures. The storage modulus, G', and the loss modulus, G'', for the dispersions were then measured. Based on the results of the viscoelasticity measurements in the present study and the physicochemical properties of the ChNFs in our previous study [12], the nanostructural transformation associated with the progression of the chitin disintegration was surmised.

2. Experimental Section

2.1. Materials

Both α- and β-chitin were used in the present study. The α-chitin (< 100 μm in diameter, 96% *N*-acetylation) was obtained from Yaegaki Bio-industry, Inc. (Himeji, Japan) and was used without further purification. The β-chitin was prepared from squid pens (*Todarodes pacificus*) according to the method reported in our previous study [6]. In brief, the squid pens were treated with 0.1 mol L^{-1} hydrochloric acid for 16 h at 15 °C to remove ash and then twice with 1 mol L^{-1} sodium hydroxide for 2 h at 90 °C to remove protein. The purified β-chitin (95% *N*-

acetylation) was pulverized into ~100 μm particles using a dry pulverizer (Nippon Steel & Sumikin Fine Technology Co., Ltd., Cyclone Mill, Osaka, Japan). The hydrochloric acid was purchased from Wako Pure Chemical Industries (Osaka, Japan) and was used without further purification.

2.2. Preparation of ChNFs

The α- and β-chitin powders were separately suspended in distilled water at concentrations of 0.05, 0.1, 0.5, 1, and 2 w/v%. A dilute hydrochloric acid solution was added to the chitin slurries to adjust their acidity before they were disintegrated into NFs. The acidity proposed in our previous study [12], which is the molar ratio of the protons dissociated from the acid to the amino groups in the chitin, is effective for controlling the physicochemical properties of α- and β-ChNFs. The acidities of the β-ChNF slurries were set to 0 and 0.93 mol mol^{-1}, which produced the minimum and maximum viscosities, respectively, for the β-ChNFs that were disintegrated by 10 collisions with ceramic balls, as described below. The acidities of the α-ChNF slurries were set to a wider range of 0, 0.38, and 1.55 mol mol^{-1} because the influence of the acidity on the physicochemical properties of the α-ChNFs was minimal, as we have reported previously [12]. In the present study, for a given acidity, the ChNFs were expressed as ChNFs [x], where x is the acidity. The chitin slurries were disintegrated using a Star Burst system (Star Burst Mini, Sugino Machine Co., Ltd., Uozu, Japan) equipped with a ball-collision chamber. The chitin slurries, pressurized to approximately 235 MPa, were ejected from the nozzle (100 μm aperture) such that they collided with a ceramic ball. The disintegrated samples were cooled to 25 °C by passing them through a heat exchanger before being recovered. The number of collisions with the ceramic balls (i.e., passes) was set to 2, 5, or 10.

2.3. Dynamic Viscoelastic Measurements

The disintegrated samples were defoamed to inhibit bubble generation during the measurements. Dispersions of < 0.1 w/v% α- and β-ChNFs were heated to 30 °C using a thermostatic water bath and were then sonicated at 30 °C for 5 min with an ultrasonic washing machine under a 0.02 MPa vacuum. The dispersions of > 0.5 w/v% α- and β-ChNFs were heated to 40 °C using the thermostatic water bath and were stirred at 1000 rpm for 1 min and then defoamed at 1000 rpm for 1 min using a mixer (ARE-250, Thinky Co., Ltd., Tokyo, Japan). Dynamic viscoelasticity measurements were carried out using a coaxial double-cylinder rheometer (Rheologia Agent A300, Elquest Co., Ltd., Chiba, Japan) equipped with a thermostatic water bath set to 25 °C (Fig. 1). The gap between the cylinders was approximately 1.1 mm. The linear viscoelastic region was determined by strain γ sweep measurements for all the samples before the angular frequency ω sweep measurements. The γ sweep measurement was carried out in the range 0.01–10% at an ω setting of 1.26 s^{-1}. The ω sweep measurement was carried out in the range 0.0628–62.9 s^{-1} while γ was set to 0.02% for both the 0.5 w/v% dispersion of β-ChNFs [0.93] and the > 1 w/v% dispersions of α- and β-ChNFs, and to 0.07% for the other samples.

3. Results and Discussion

3.1. The linear viscoelastic region and the sol-gel transition from strain sweep measurements

The apparent transmittance and viscosity of the β-ChNFs [0.93] were considerably greater than those of the β-ChNFs [0], and those of α-ChNFs were slightly affected by increases in the acidity, as reported in our previous study [12]. The pH of the α- and β-ChNFs changed depending on the number of passes, as summarized in Table S1. The G' and G'' values for each pass of the α- and β-ChNF dispersions prepared at various concentrations and acidities are plotted as a function of the strain, γ, and these results are presented in Fig. S1. First, we

determined the linear viscoelastic region for γ, as described in section 2.3. Next, we focused on the sol-gel transition (i.e., the point at which $G'' > G'$) upon the application of strain. For a dispersion of < 0.1 w/v%, the results calculated from the representative data are shown in Fig. 2a. The γ value at the sol-gel transition for the α- and β-ChNFs [0] was 1–2%, and that at the sol-gel transition for the α-ChNFs [1.55] and β-ChNFs [0.93] was either around 0.5% or could not be defined (i.e., $G'' > G'$ for the measured values of γ). At concentrations > 0.5 w/v%, the results calculated from the representative data are shown in Fig. 2b. The γ value at the sol-gel transition for the α- and β-ChNFs [0] was around 0.5% and that at the sol-gel transition for the α-ChNFs [1.55] and β-ChNFs [0.93] was 0.1–0.2%. The sol-gel transitions in the acidic pH occurred at a lower γ value than those at the neutral pH because the cationization of the ChNF surface under acidic conditions leads to electrostatic repulsion between the ChNFs, so fraying would progress as a result of the application of strain. In addition, G'' slightly increased for the > 0.5 w/v% β-ChNFs [0.93] and α-ChNFs [1.55] immediately before the sol transition shown in Fig. 2b, represented by open diamonds and open triangles, respectively. At the low-strain region before the increase in G'', the energy applied as a result of the strain was mostly absorbed by the network structure. The presence of a highly entangled structure was assumed for the ChNF dispersions. Actually, these ChNF dispersions did not readily flow when the container was tilted. A subsequent increase in G'' resulted in the network structure fraying and transitioning to the sol state. Furthermore, G'' decreased with the application of small amounts of energy because the ChNFs easily flowed owing to their disentangled network structures.

3.2. Nanostructural evaluations based on angular frequency sweep measurements

The G' and G'' values for each pass of the α- and β-ChNF dispersions prepared at various concentrations are plotted as a function of the angular frequency, ω, in Fig. S2. For the α-ChNFs [0] and β-ChNFs [0] dispersions, the results calculated from the representative data are

shown in Fig. 3a. The G' values were almost independent of ω (i.e., $G' \propto \omega^0$) regardless of the number of passes or the concentration, and the loss angle (i.e., tan $\delta = G'' / G'$) was 0.15–0.2 for the α-ChNFs [0] and 0.1–0.15 for the β-ChNFs [0], indicating that a very large network structure was formed and that the NFs did not relax. For the α-ChNFs [1.55] and β-ChNFs [0.93] dispersions, the results calculated from the representative data are shown in Fig. 3b. The 0.05 w/v% dispersions of α-ChNFs [1.55] and β-ChNFs [0.93] exhibited a colloidal state; that is, $G'' > G'$ for the measured values of ω, indicating that there were few entanglements between the ChNFs. The 0.1 w/v% dispersions of α-ChNFs [1.55] and β-ChNFs [0.93] often exhibited the critical gel state; that is, G' and $G'' \propto \omega^n$ ($0 < n < 1$), indicating that the dispersions were transitioning from a sol into a gel. The number of entanglement points increased owing to the increase in the number of NFs such that a vast cluster was just formed. The dispersions above 0.5 w/v% exhibited elastic behavior, with tan δ being 0.1–0.15 for the α-ChNFs [1.55] and β-ChNFs [0.93], indicating that a network structure had developed.

3.3. Effects of concentration dependence of G′ on the fractal dimensions of the network structure

The concentration dependence of G' at $\omega = 1.26$ s^{-1} for each pass of the α- and β-ChNF dispersions prepared at various acidities is shown in Fig. 4. The least-squares method (i.e., exponential concentrations) was used to produce regression lines whose slopes are summarized in Table 1. A scaling law linking G' and the NF concentration (c) has been proposed [16,17]:

$$G' \propto c^{(3+D_F)/(3-D_F)}$$

where D_F is the fractal dimension of the object-connecting junctions. According to this relation, the D_Fs of the pH neutral ChNF dispersions are 0.8–1.1, and those of the acidic ChNF dispersions are 1.5–1.8, indicating that the aggregate formed by the entanglement of the pH neutral ChNFs was quasilinear. The aggregate formed by the entanglement of the acidified

ChNFs, on the other hand, formed a complex linear pattern spreading in a plane. Further, another relation between G' and c has been proposed [18]:

$$G' \propto kc^{\alpha}$$

where k is a front factor proportional to the Young's modulus and the square of the aspect ratio of a single fiber, and α is the characteristic of the network structure. The value of α is 1–1.5 for a longitudinally directed fiber network (perpendicular to the plates of the rheometer), 2.25 for a random 3D network structure, and 3–4 for a laminated 2D network structure (parallel to the plates of the rheometer). From the values listed in Table 1, α increased with increasing number of passes and acidity. The nanostructures of the pH neutral ChNF dispersions more closely approached that of a random 3D network as the disintegration progressed. For the acidified ChNF dispersions, the nanostructures changed into laminated 2D networks after only 2 passes, and α increased further to almost 4 with subsequent passes.

3.4. Disintegration of ChNFs as a function of both G′ and the number of passes

The dependence of G' on the number of passes was confirmed with the > 0.5 w/v% dispersions of α- and β-ChNFs, which have a well-developed network structure (Fig. 5). The number of passes of the β-ChNFs [0] did not significantly affect G'. In our previous study, the viscosity of the β-ChNF [0] dispersion did not change even when the number of passes was increased [12]. Furthermore, in the present study, the G' value of the β-ChNFs [0] was unrelated to the number of passes. Further study is required to determine the reason for this. The β-ChNFs [0.93] exhibited their largest value of G' after only two passes, but G' decreased between five and ten passes. The decrease in G' was due to the decrease in the aspect ratio (i.e., length/width) of the β-ChNFs. Several reports have addressed the decrease in the aspect ratio of the acidified and excessively disintegrated β-ChNFs [12,14,19]. On the other hand, the G' value for the α-ChNFs increased with increasing number of passes (particularly between two and five passes)

regardless of the pH. This result indicates that the disintegration of the α-chitin had progressed continuously, most likely because the massive number of hydrogen bonds in α-chitin causes a much stronger interaction between NFs.

3.5. Nanostructural transformation associated with the disintegration progress

We assumed that the β-ChNFs in acidic conditions were mostly individualized because we found in our previous study [12] that the transmittance was in excess of 70% after as few as two passes and was around 95% after ten passes. Compared to all of the ChNF series that we considered, β-ChNFs in acidic conditions reached the highest viscosity (around 3600 mPa s). Although the 0.05 w/v% β-ChNFs [0.93] did not show a sufficiently entangled structure to exhibit elastic behavior, they were dispersed, forming a nematic liquid crystalline phase rather than a lone state [14]. When the individualized ChNFs did not stabilize at an entanglement point and became ordered with a nematic arrangement, the number of entanglement points massively increased with increasing concentration. Thus, the dispersion of >0.5 w/v% β-ChNFs [0.93] exhibited the greatest G' value among the ChNF series being considered. Even when the aspect ratio decreased with excessive disintegration, the network structure was maintained, and the β-ChNFs still exhibited a G' value greater than that of the other ChNFs that were passed 10 times.

The disintegration progress of the α- and β-ChNFs [0] showed similar behavior according to the viscoelasticity measurements. Although these ChNFs exhibited elastic behavior under almost all conditions, the behavior of the individualized ChNFs did not appear in the slope of the scaling law (i.e., their slope limited at approximately 2). In addition, these ChNFs were opaque with a low viscosity as reported previously [12], so they had not been disintegrated to the point where they existed as individual nanofibers. These characteristics of the pH neutral ChNFs were likely due to particulate chitin remnants. The purified chitin particles have a tightly assembled structure formed by the strong secondary interactions among the ChNFs.

After disintegrating them with the Star Burst system, some of the assembled structure would remain. Because the framework of the assembled structure consisted of yoked ChNFs, any stress was easily transmitted to the framework. On the other hand, the number of entanglement points between such inadequately disintegrated regions slightly increased with increasing concentration because these inadequately disintegrated regions could not percolate into other regions and would become entangled at the only surfaces. The relatively small fractal dimensions support the above scenario. In our previous study, the α-chitin did not disintegrate as readily as the β-chitin, and the transmittance and viscosity of the α-ChNFs were lower than those of the β-ChNFs [12]. Thus, there would have been many more inadequately disintegrated regions than for the β-ChNFs. As a result, the G' value of α-ChNFs [0] was smaller than that of β-ChNFs [0].

Finally, many aspects of the disintegration progress of α-ChNFs [1.55] remain unclear. In our previous study, the transmittance and viscosity of the α-chitin slightly increased as a result of acidifying the dispersion [12]. We thought that the results obtained for the α-ChNFs [1.55] would be similar to those obtained for the α-ChNFs [0]. However, the results suggested that the dispersion of the α-ChNFs [1.55] transitioned from a colloidal state to elastic behavior and showed a nematic liquid crystalline phase with increasing α-ChNF [1.55] concentration. Because the α-ChNF [1.55] dispersion displayed such characteristics, its transmittance should have been more than 90%; however, the dispersions were actually opaque regardless of the degree of disintegration [12]. Further analysis such as neutron scattering and X-ray scattering of the bulk dispersions rather than electron microscopy of localized regions is needed to provide more insight into the disintegration behavior of α- and β-ChNFs [0] as mentioned above and to clarify the disintegration progression for acidified α-ChNFs.

3.6. Comparison of our ChNF viscoelastic results to previous chitin and NF studies

Some reports have addressed the dynamic viscoelasticity measurements of chitin solutions before the high-aspect-ratio chitin NFs were measured. The G' and G'' values of 3 wt.% chitin dissolved in an *N*, *N*-DMAc(dimethylacetamide)/LiCl solution at 30 °C are –0.3 Pa and 5.5 Pa [20], respectively. The G' value for 3.2 w/v% chitin dissolved in an ionic liquid (1-butyl-3-methylimidazolium acetate) is 1 Pa while $G'' > G'$ [21]. The G' value for 1 wt% chitin dissolved in urea/NaOH is 10^{-2} Pa while $G'' > G'$ [22]. According to these previous studies, 1–3% chitin solutions exhibit $G'' > G'$ over a wide ω range while the G' value is several Pa. In addition, the dynamic viscoelasticity of nanorods or nanowhiskers prepared by acid hydrolysis has been reported. The G' value of 2.4 wt% chitin nanorods (aspect ratio = 13.5) prepared by acid hydrolysis with 3 N hydrochloric acid is 1 Pa, where $G'' > G'$ [23]. The G' values of 1 and 3 wt.% cellulose nanorods (aspect ratio = 42) prepared by acid hydrolysis with 4 N hydrochloric acid are 7 and 60 Pa, respectively [24]. In the present study, the G' values for the 1 and 2 w/v% β-ChNFs [0.93] were 300 and 1000 Pa, respectively, after two passes. ChNFs that disintegrate as a result of mechanical shear force often exhibit a higher aspect ratio [7,25,26]. When thinner and longer NFs exist in the dispersion, the degree of entanglement can increase. As a result, the G' value for the ChNF dispersion was greater than that of either a chitin solution or chitin nanorods.

Other studies have reported the results of viscoelasticity measurements for neutral α-ChNFs disintegrated by various numbers of passes with an Aqueous Counter Collision system (similar to the Star Burst system) [15]. The G' value for a 0.4 wt% dispersion of neutral α-ChNFs after ten passes is 20 Pa. The G' values for 1 and 2 wt% cellulose NF dispersions disintegrated by a high-pressure homogenizer after enzymatic hydrolysis are 100 and 2000 Pa, respectively [17]. The G' value for these NFs is almost the same as that for the same concentration of NFs prepared using mechanical disintegration. The G' value for 0.1 wt% bacterial cellulose NFs (with aspect ratios in the range 220–450) produced by acetobacter, on

the other hand, is 10 Pa [24]. The G' values for 1% (2,2,6,6-tetramethylpiperidin-1-yl)oxyl-(TEMPO)-oxidized cellulose NFs having degrees of polymerization of 100 and 500 are 250 and 1000 Pa, respectively [27]. The 0.1% TEMPO-oxidized, high-aspect-ratio cellulose NFs exhibit critical gelation. These high-aspect-ratio NFs exhibit G' values greater than those of mechanically disintegrated NFs. When researchers undertake material design utilizing NFs, therefore, it is important to consider both the NF aspect ratio and G' values.

5. Conclusions

Concentration, disintegration time, acidity, and crystalline structure are all important factors affecting the dispersibility of ChNFs. Dynamic viscoelasticity measurements were carried out for ChNFs under a range of conditions to reveal the nanostructural transformation associated with the disintegration progress. In the strain-sweep measurements used to confirm the linear region (i.e., strain vs. stress), the sol-gel transition was produced by less strain in the acidified ChNFs, indicating that the electrostatic repulsion between the ChNFs disentangled the knotted ChNFs at low strain. The changes in the storage modulus, as determined by the frequency-sweep measurements, for a given angular frequency, concentration, and number of passes, indicated the disintegration progress of the neutral and acidified α- and β-ChNFs. The 0.05 w/v% dispersion of β-ChNFs [0.93] transitioned from a colloidal state into a critical gel state and showed elastic behavior with increasing β-ChNF concentration, suggesting the existence of individualized β-ChNFs [0.93] in the dispersion. Although these ChNFs did not intertangle well at low concentrations, a network structure developed at high concentrations. From the scaling law linking G' and ChNF concentration, the fractal dimension was found to be 3–4, and the nanostructure was a nematic liquid crystalline phase. In addition, the decrease in the aspect ratio of the β-ChNFs [0.93] was caused by excessive disintegration. The β-ChNFs [0] exhibited elastic behavior even at a low concentration (i.e., 0.05 w/v%). The fractal

dimension was around 1, and the nanostructure transitioned from an intermediate structure into a random 3D network; thus, the β-ChNFs [0] did not individualize. The elastic behavior could be the result of the slight entanglement between the inadequately disintegrated regions in which some assembled structure remained. The results obtained for the α-ChNFs [0] were similar to those obtained for the β-ChNFs [0]. Because the α-ChNFs [0] were bound to the inadequately disintegrated region owing to the relatively strong secondary interactions, the G' value of the α-ChNFs [0] was smaller than that of the β-ChNFs [0]. In addition, the α-ChNFs [0] steadily disintegrated with an increase in the number of passes. Moreover, the ChNF dispersions prepared in the present study exhibited more elastic behavior than a chitin solution of the same concentration, indicating that the ChNFs were very intertangled. A better understanding of the rheology properties of ChNF dispersions will enhance the success of material design using ChNFs.

Acknowledgements

This work was supported by JSPS KAKENHI [grant number 17H04893]. We thank Dr. Nobuhide Takahashi, Dr. Hiroshi Fukunaga, Dr. Iori Shimada, Dr. Kazuhide Totani, Dr. Yoshihiro Nomura, and Mr. Kazuhiko Yamashita for important intellectual contribution to the conception of the project.

References

[1] Y. Ogawa, R. Hori, U.J. Kim, M. Wada, Elastic modulus in the crystalline region and the thermal expansion coefficients of α-chitin determined using synchrotron radiated X-ray diffraction, Carbohydr. Polym. 83 (2011) 1213–1217. doi:10.1016/j.carbpol.2010.09.025.

[2] L. Liu, R. Wang, J. Yu, J. Jiang, K. Zheng, L. Hu, Z. Wang, Y. Fan, Robust Self-Standing Chitin Nanofiber/Nanowhisker Hydrogels with Designed Surface Charges and Ultralow Mass Content via Gas Phase Coagulation, Biomacromolecules. 17 (2016) 3773–3781. doi:10.1021/acs.biomac.6b01278.

[3] R. Jayakumar, V.V. Divya Rani, K.T. Shalumon, P.T.S. Kumar, S.V. Nair, T. Furuike, H. Tamura, Bioactive and osteoblast cell attachment studies of novel α- and β-chitin membranes for tissue-engineering applications, Int. J. Biol. Macromol. 45 (2009) 260–264. doi:10.1016/j.ijbiomac.2009.06.002.

[4] B.M. Min, S.W. Lee, J.N. Lim, Y. You, T.S. Lee, P.H. Kang, W.H. Park, Chitin and chitosan nanofibers: Electrospinning of chitin and deacetylation of chitin nanofibers, Polymer (Guildf). 45 (2004) 7137–7142. doi:10.1016/j.polymer.2004.08.048.

[5] M. Paillet, A. Dufresne, Chitin whisker reinforced thermoplastic nanocomposites, Macromolecules. 34 (2001) 6527–6530. doi:10.1021/ma002049v.

[6] S. Suenaga, N. Nikaido, K. Totani, K. Kawasaki, Y. Ito, K. Yamashita, M. Osada, Effect of purification method of β-chitin from squid pen on the properties of β-chitin nanofibers, Int. J. Biol. Macromol. 91 (2016) 987–993.

doi:10.1016/j.ijbiomac.2016.06.060.

[7] C. Chen, D. Li, Q. Hu, R. Wang, Properties of polymethyl methacrylate-based nanocomposites: Reinforced with ultra-long chitin nanofiber extracted from crab shells, Mater. Des. 56 (2014) 1049–1056. doi:10.1016/j.matdes.2013.11.057.

[8] M. Kawata, K. Azuma, H. Izawa, M. Morimoto, H. Saimoto, S. Ifuku, Biomineralization of calcium phosphate crystals on chitin nanofiber hydrogel for bone regeneration material, Carbohydr. Polym. 136 (2015) 964–969. doi:10.1016/j.carbpol.2015.10.009.

[9] K. Abe, S. Ifuku, M. Kawata, H. Yano, Preparation of tough hydrogels based on β-chitin nanofibers via NaOH treatment, Cellulose. 21 (2014) 535–540. doi:10.1007/s10570-013-0095-0.

[10] P. Ang-atikarnkul, A. Watthanaphanit, R. Rujiravanit, Fabrication of cellulose nanofiber/chitin whisker/silk sericin bionanocomposite sponges and characterizations of their physical and biological properties, Compos. Sci. Technol. 96 (2014) 88–96. doi:10.1016/j.compscitech.2014.03.006.

[11] Y. Lu, Q. Sun, X. She, Y. Xia, Y. Liu, J. Li, D. Yang, Fabrication and characterisation of α-chitin nanofibers and highly transparent chitin films by pulsed ultrasonication, Carbohydr. Polym. 98 (2013) 1497–1504. doi:10.1016/j.carbpol.2013.07.038.

[12] S. Suenaga, K. Totani, Y. Nomura, K. Yamashita, I. Shimada, H. Fukunaga, N. Takahashi, M. Osada, Effect of acidity on the physicochemical properties of α- and β-chitin nanofibers, Int. J. Biol. Macromol. 102 (2017) 358–366. doi:10.1016/j.ijbiomac.2017.04.011.

[13] N.E. Mushi, J. Kochumalayil, N.T. Cervin, Q. Zhou, L.A. Berglund, Nanostructurally

Controlled Hydrogel Based on Small-Diameter Native Chitin Nanofibers: Preparation, Structure, and Properties, ChemSusChem. 9 (2016) 989–995. doi:10.1002/cssc.201501697.

[14] M. Yokoi, R. Tanaka, T. Saito, A. Isogai, Dynamic Viscoelastic Functions of Liquid-Crystalline Chitin Nanofibril Dispersions, Biomacromolecules. 18 (2017) 2564–2570. doi:10.1021/acs.biomac.7b00690.

[15] R. Kose, T. Kondo, Favorable 3D-network Formation of Chitin Nanofibers Dispersed in Water Prepared Using Aqueous Counter Collision, Sen'i Gakkaishi. 67 (2011) 91–95. doi:10.2115/fiber.67.91.

[16] J.-M. Guenet, Structure versus rheological properties in fibrillar thermoreversible gels from polymers and biopolymers, J. Rheol. (N. Y. N. Y). 44 (2000) 947–960. doi:10.1122/1.551121.

[17] M. Pääkko, M. Ankerfors, H. Kosonen, A. Nykänen, S. Ahola, M. Österberg, J. Ruokolainen, J. Laine, P.T. Larsson, O. Ikkala, T. Lindström, Enzymatic hydrolysis combined with mechanical shearing and high-pressure homogenization for nanoscale cellulose fibrils and strong gels, Biomacromolecules. 8 (2007) 1934–1941. doi:10.1021/bm061215p.

[18] L. Yu, D. Tatsumi, M. Morita, Relationship between Viscoelasticity and Electrical Conductivity of Carbonized Cellulose Fiber Networks, Nihon Reoroji Gakkaishi. 41 (2013) 331–336.

[19] A.K. Dutta, H. Izawa, M. Morimoto, H. Saimoto, S. Ifuku, Simple Preparation of Chitin Nanofibers from Dry Squid Pen β-chitin Powder by the Star Burst System, J. Chitin Chitosan Sci. 1 (2013) 186–191. doi:10.1166/jcc.2013.1023.

[20] B. Chen, K. Sun, K. Zhang, Rheological properties of chitin/lithium chloride, N, N-dimethyl acetamide solutions, Carbohydr. Polym. 58 (2004) 65–69. doi:10.1016/j.carbpol.2004.06.030.

[21] J.I. Horinaka, Y. Urabayashi, T. Takigawa, M. Ohmae, Entanglement network of chitin and chitosan in ionic liquid solutions, J. Appl. Polym. Sci. 130 (2013) 2439–2443. doi:10.1002/app.39459.

[22] X. Hu, Y. Du, Y. Tang, Q. Wang, T. Feng, J. Yang, J.F. Kennedy, Solubility and property of chitin in NaOH/urea aqueous solution, Carbohydr. Polym. 70 (2007) 451–458. doi:10.1016/j.carbpol.2007.05.002.

[23] M.V. Tzoumaki, T. Moschakis, C.G. Biliaderis, Metastability of nematic gels made of aqueous chitin nanocrystal dispersions, Biomacromolecules. 11 (2010) 175–181. doi:10.1021/bm901046c.

[24] D. Tatsumi, S. Ishioka, T. Matsumoto, Effect of Fiber Concentration and Axial Ratio on the Rheological Properties of Cellulose Fiber Suspensions, Nihon Reoroji Gakkaishi. 30 (2002) 27–32. doi:10.1678/rheology.30.27.

[25] Y. Fan, T. Saito, A. Isogai, Preparation of chitin nanofibers from squid Pen β-chitin by simple mechanical treatment under acid conditions, Biomacromolecules. 9 (2008) 1919–1923. doi:10.1021/bm800178b.

[26] S. Ifuku, M. Nogi, M. Yoshioka, M. Morimoto, H. Yano, H. Saimoto, Fibrillation of dried chitin into 10-20 nm nanofibers by a simple grinding method under acidic conditions, Carbohydr. Polym. 81 (2010) 134–139.

doi:10.1016/j.carbpol.2010.02.006.

[27] K. Benhamou, A. Dufresne, A. Magnin, G. Mortha, H. Kaddami, Control of size and viscoelastic properties of nanofibrillated cellulose from palm tree by varying the TEMPO-mediated oxidation time, Carbohydr. Polym. 99 (2014) 74–83. doi:10.1016/j.carbpol.2013.08.032.

Appendix A. Supplementary Data

Supplementary data associated with this article can be found in the online version at.

Tables

Table 1. Slopes of linear regressions on a double-logarithmic chart of concentration vs. storage modulus G' for α- and β-ChNFs prepared with different numbers of passes and acidities

Passes	β-ChNFs [0]	β-ChNFs [0.93]	α-ChNFs [0]	α-ChNFs [0.38]	α-ChNFs [1.55]
2	1.8	3.1	1.8	2.2	3.0
5	1.9	3.5	1.8	2.2	3.2
10	2.1	3.6	1.9	2.6	4.2

Figure Captions

Fig. 1. Coaxial double-cylinder rheometer with thermostatic water bath.

Fig. 2. A double logarithmic plot of storage modulus (G') and loss modulus (G'') data as a function of strain (γ) for α- and β-ChNFs: (a) 0.1 w/v% and 10 passes (b) 0.5 w/v% and 10 passes.

Fig. 3. A double logarithmic plot of storage modulus (G') and loss modulus (G'') data as a function of angular frequency (ω) for α- and β-ChNFs: (a) neutral condition and 5 passes (b) acidic condition and 5 passes.

Fig. 4. Storage modulus (G') measured at $\omega = 1.26\ s^{-1}$ plotted as a function of concentration for α- and β-ChNFs prepared with different numbers of passes and acidities.

Fig. 5. Storage modulus (G') measured at $\omega = 1.26\ s^{-1}$ plotted as a function of the number of passes for α- and β-ChNFs prepared at concentrations over 0.5 w/v% and different acidities.

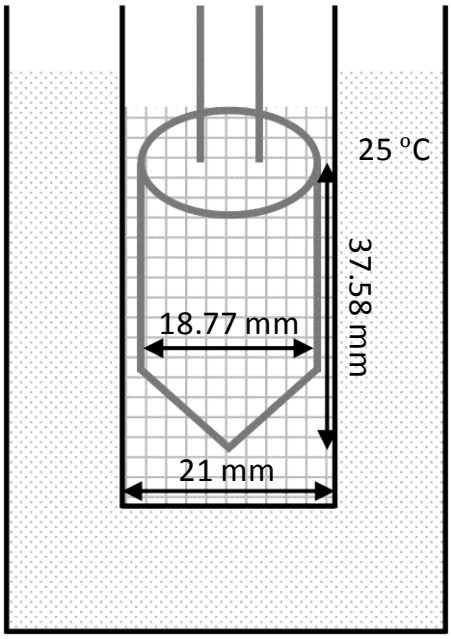

Fig. 1. Coaxial double-cylinder rheometer with thermostatic water bath.

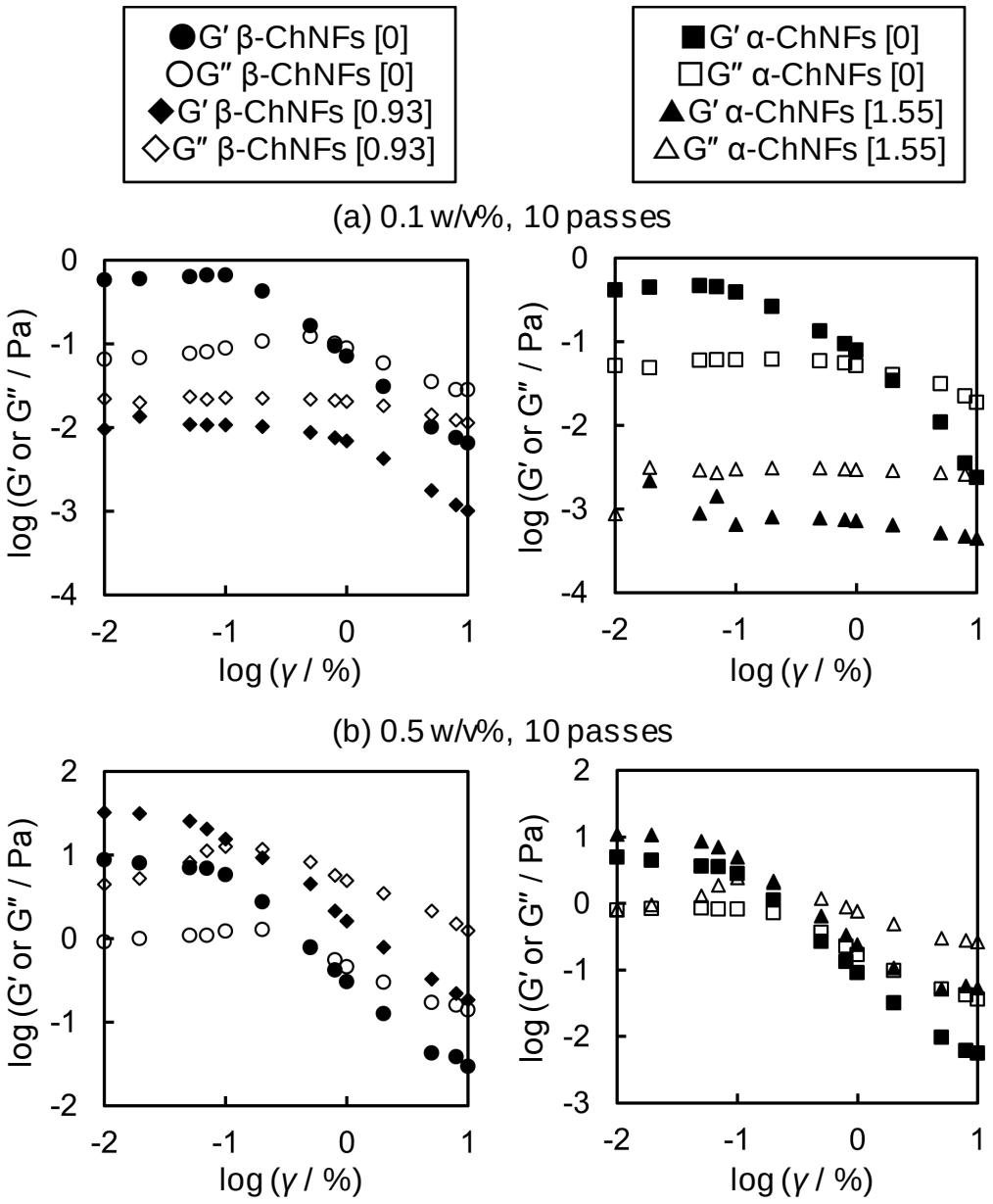

Fig. 2. A double logarithmic plot of storage modulus (G') and loss modulus (G'') data as a function of strain (γ) for α- and β-ChNFs: (a) 0.1 w/v% and 10 passes (b) 0.5 w/v% and 10 passes.

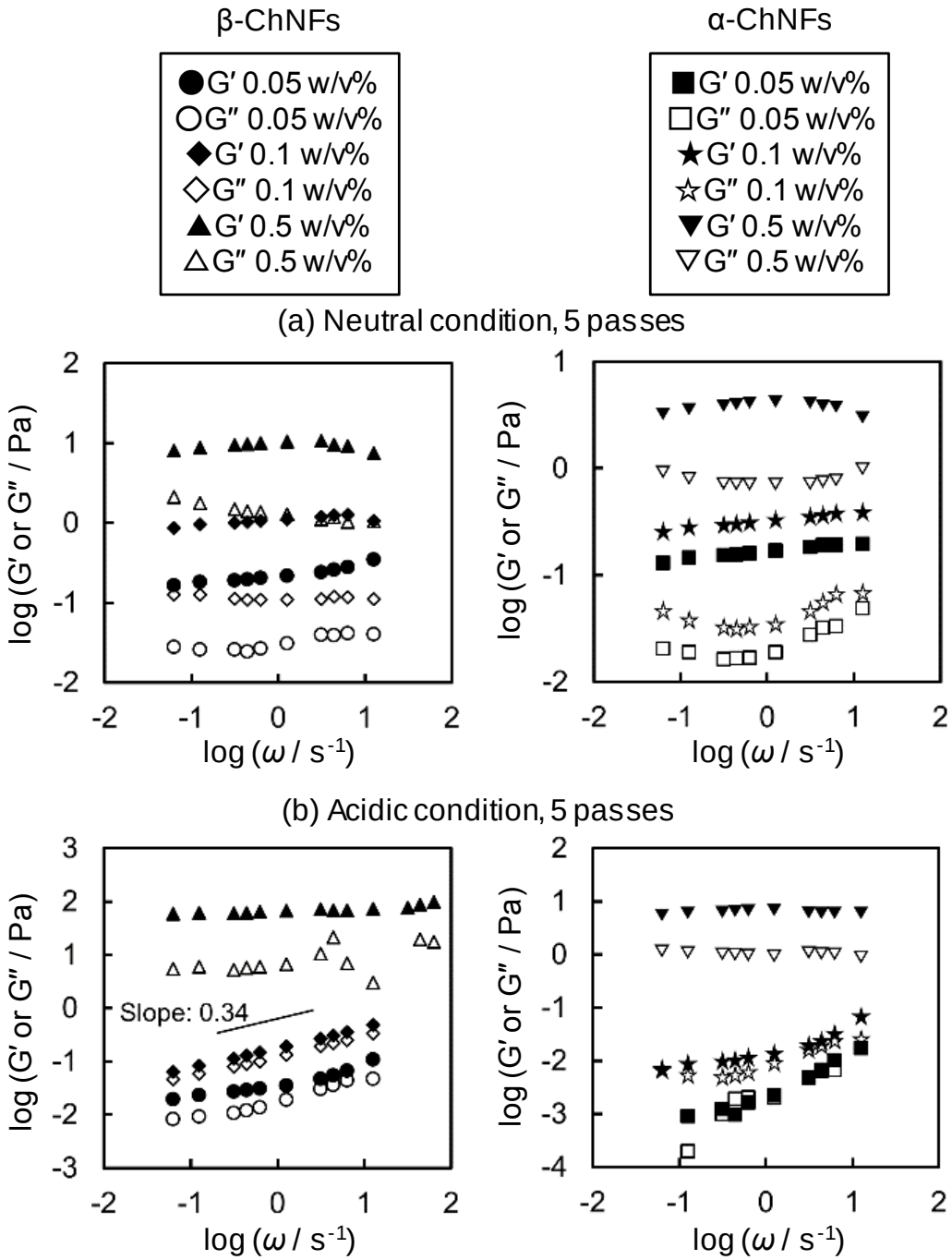

Fig. 3. A double logarithmic plot of storage modulus (G') and loss modulus (G'') data as a function of angular frequency (ω) for α- and β-ChNFs: (a) neutral condition and 5 passes (b) acidic condition and 5 passes.

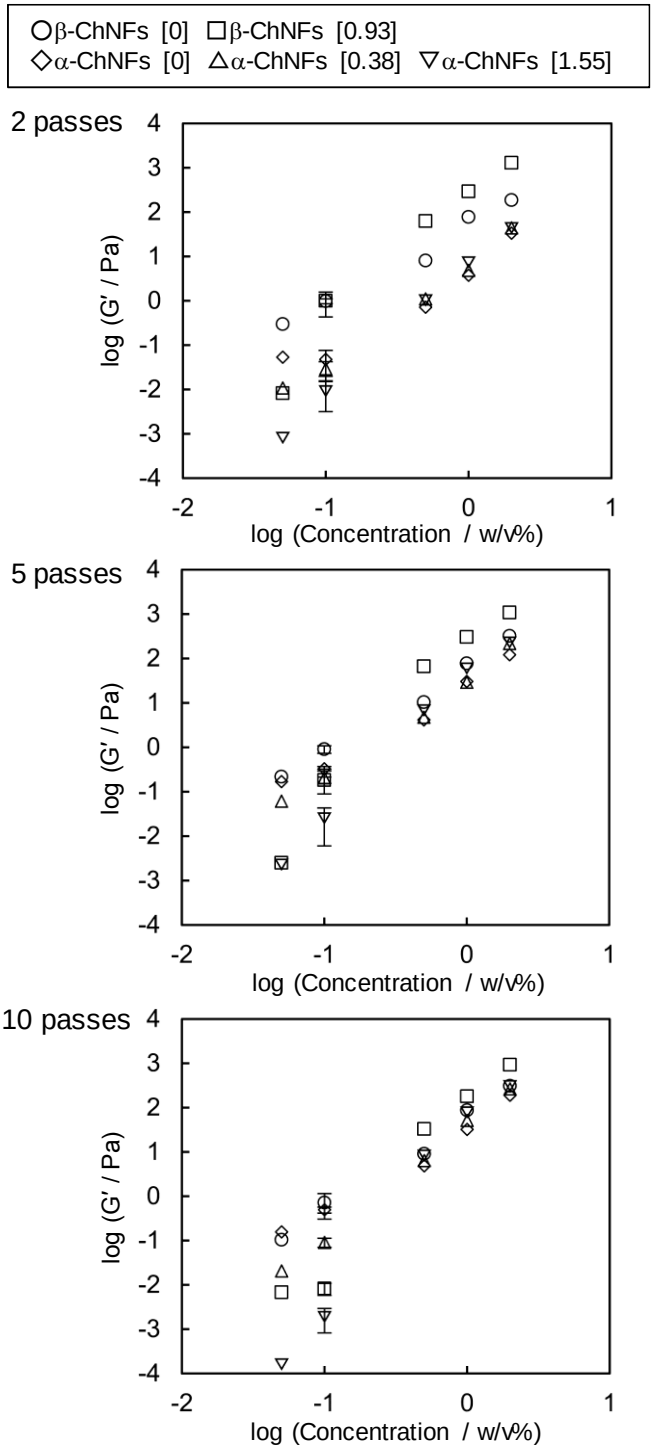

Fig. 4. Storage modulus (G') measured at $\omega = 1.26$ s^{-1} plotted as a function of concentration for α- and β-ChNFs prepared with different numbers of passes and acidities.

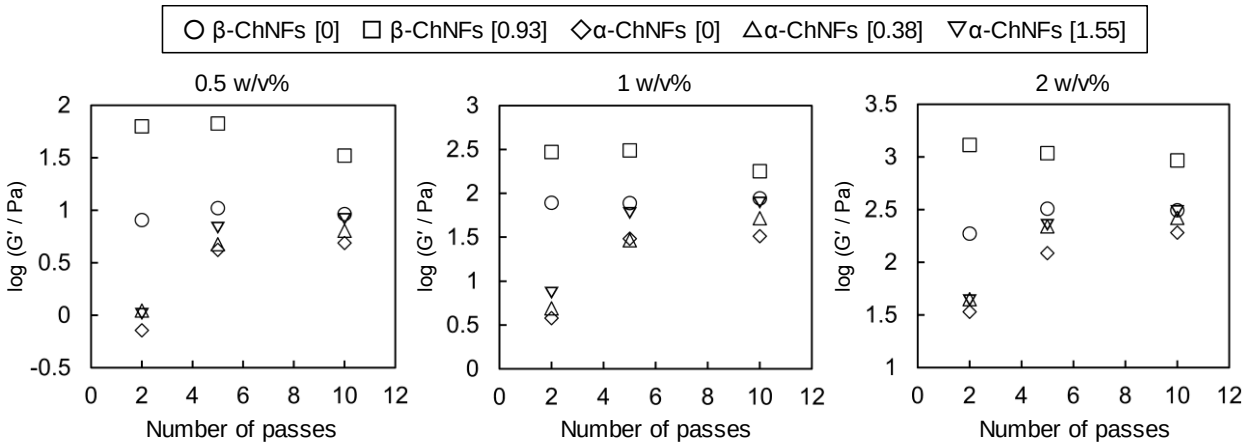

Fig. 5. Storage modulus (G') measured at $\omega = 1.26\ s^{-1}$ plotted as a function of the number of passes for α- and β-ChNFs prepared at concentrations over 0.5 w/v% and different acidities.